

The Yeast Alix Homolog Bro1 Functions as a Ubiquitin Receptor for Protein Sorting into Multivesicular Endosomes

Natasha Pashkova,¹ Lokesh Gakhar,² Stanley C. Winistorfer,¹ Anna B. Sunshine,⁴ Matthew Rich,⁴ Maitreya J. Dunham,⁴ Liping Yu,³ and Robert C. Piper^{1,*}

¹Department of Molecular Physiology and Biophysics

²Crystallography Facility, Carver College of Medicine

³Nuclear Magnetic Resonance Facility, Carver College of Medicine

University of Iowa, Iowa City, IA 52242, USA

⁴Department of Genome Sciences, University of Washington, Seattle, WA 98195, USA

*Correspondence: robert-piper@uiowa.edu

<http://dx.doi.org/10.1016/j.devcel.2013.04.007>

SUMMARY

Sorting of ubiquitinated membrane proteins into luminal vesicles of multivesicular bodies is mediated by the Endosomal Sorting Complex Required for Transport (ESCRT) apparatus and accessory proteins such as Bro1, which recruits the deubiquitinating enzyme Doa4 to remove ubiquitin from cargo. Here we propose that Bro1 works as a receptor for the selective sorting of ubiquitinated cargos. We found synthetic genetic interactions between *BRO1* and ESCRT-0, suggesting that Bro1 functions similarly to ESCRT-0. Multiple structural approaches demonstrated that Bro1 binds ubiquitin via the N-terminal trihelical arm of its middle V domain. Mutants of Bro1 that lack the ability to bind Ub were dramatically impaired in their ability to sort Ub-cargo membrane proteins, but only when combined with hypomorphic alleles of ESCRT-0. These data suggest that Bro1 and other Bro1 family members function in parallel with ESCRT-0 to recognize and sort Ub-cargos.

INTRODUCTION

Ubiquitin (Ub) is a sorting determinant mediating the degradation of a wide variety of membrane proteins in lysosomes by sorting them into the intraluminal vesicles (ILVs) of multivesicular endosomes/bodies (MVBs) (Hanson and Cashikar, 2012). Ub is recognized by the ESCRT (Endosomal Sorting Complex Required for Transport) apparatus, which couples cargo recognition and sorting with the formation and scission of intraluminal vesicles (Henne et al., 2011). Recognition of ubiquitinated cargo (Ub-cargo) occurs early during ILV formation and is mediated in large part by ESCRT-0 and ESCRT-I, which each have multiple Ub-binding domains (UBDs) (Clague et al., 2012; Shields and Piper, 2011). ESCRT-0, composed of Vps27 and Hse1 in yeast and by Hrs and STAM1/2 in humans, binds Ub via multiple UBDs housed within its Vps27/Hrs/Stam (VHS) and Ubiquitin

Interacting Motif domains. ESCRT-0 is thought to be the endosomal Ub-sorting receptor that initiates cargo capture and has a variety of protein interactions that equip it for this task. Direct binding to clathrin positions it within clathrin-enriched endosomal subdomains where cargo is segregated for recycling or degradation. ESCRT-0 also binds ESCRT-I to facilitate assembly of the ESCRT apparatus and the transfer of Ub-cargo to ESCRT-I and -II. ESCRT-0 also associates with both Ub ligases and deubiquitinating enzymes (DUBs) that may alter cargo ubiquitination and regulate its sorting into the MVB pathway. Several other proteins are proposed to work in parallel to ESCRT-0 as alternative ESCRT-0-like Ub-sorting receptors (Clague et al., 2012; Shields and Piper, 2011). Among these are the Tom1:Tollip complex and GGA3. Like the two subunits of ESCRT-0, both Tom1 and GGA3 have VHS domains and bind clathrin, ESCRT-I, and Ub. Functional studies implicate these as endosomal Ub-sorting receptors, although their site(s) of action and the repertoire of cargo substrates have yet to be clarified.

Late in the sorting process, ILVs are separated from the limiting membrane of the endosome by ESCRT-III, a heteropolymeric assembly of subunits centered on Snf7/CHMP4 (Babst et al., 2011). Yeast Snf7 also binds to Bro1, which in turn recruits the DUB Doa4 to remove Ub from cargo prior to its entry into ILVs (Kim et al., 2005; Luhtala and Odorizzi, 2004; Richter et al., 2007). Loss of Doa4 causes Ub to hyperaccumulate in the vacuole lumen and be depleted from the cytosol (Amerik et al., 2000; Ren et al., 2008). The Bro1:Doa4 complex is thought to work late in the sorting process, since earlier removal of Ub would permit cargo to escape incorporation into ILVs. However, loss of Bro1 produces a phenotype similar to loss of ESCRTs, while loss of Doa4 does not, demonstrating that Bro1 provides functions beyond the recruitment of Doa4 (Odorizzi et al., 2003; Raymond et al., 1992; Springael et al., 2002). Bro1 belongs to a larger family of related proteins, including mammalian Alix and HD-PTP, which share a common architecture, bind ESCRT-I, and have both an N-terminal Bro1 homology domain that binds the ESCRT-III subunit Snf7/CHMP4 and a middle V domain that, in the case of Alix, binds YPxL peptide motifs (Fisher et al., 2007; Kim et al., 2005; Lee et al., 2007). YPxL binding enables Alix to sort YPxL-bearing cargos into MVBs and to

mediate ESCRT-dependent budding of viruses that have Gag proteins bearing YPxL motifs (Baletti et al., 2012; Dores et al., 2012; Doyotte et al., 2008; Odorizzi, 2006; Sadoul, 2006; Strack et al., 2003). These data suggest that Alix and other Bro1-family proteins might recruit cargo to the ESCRT apparatus, at least along a Ub-independent pathway. Although a clear role for these proteins in the canonical sorting of Ub-cargo has not been established, recent studies have demonstrated that Alix can bind Ub, thus supporting this possibility (Joshi et al., 2008; Keren-Kaplan et al., 2013; Sangsuriya et al., 2010; Dowlatshahi et al., 2012).

Here we propose that Bro1 works in parallel with ESCRT-0 and contributes to the recognition and sorting of Ub-cargo into the MVB pathway. We show that deficiencies in Bro1 and ESCRT-0 yield synthetic phenotypes and that, like ESCRT-0, Bro1 binds clathrin. We show that the V domains of multiple Bro1 family members bind Ub and that mutations compromising Ub binding result in defective sorting of Ub-cargo.

RESULTS

Bro1 and the ESCRT-0 Ub-Sorting Receptor Interact Genetically

Deletion of either Vps27 or Hse1, two ESCRT-0 subunits (orthologous to Hrs and Stam1/2 in mammalian cells), causes a strong “class E” Vps phenotype characterized by secretion of vacuolar proteases, accumulation of large late endosomal structures, and the inability to sort ubiquitinated membrane proteins into the vacuolar lumen via the MVB pathway (Bilodeau et al., 2002). This phenotype is observed when *HSE1* is deleted from the SF838-9D parental strain but not when deleted from the SEY6210 parental strain (Figure 1A), as also noted in previous studies (Stringer and Piper, 2011). Diploid cells generated from these two *hse1Δ* strains also showed no sorting defects, providing us with a genetic tool for identifying genes that function in parallel with ESCRT-0 and whose depletion exacerbates the consequences of *HSE1* loss. The homozygous *hse1Δ* diploid was sporulated, and after one backcross to SEY6210 *hse1Δ* cells, we found that the phenotype of defective MVB sorting segregated 2:2 (Figure S1A available online). We determined the genomic sequence of the SEY6210 *hse1Δ* strain and compared it to that of *hse1Δ* segregants from a second and third backcross that showed MVB sorting defects to identify a single base-pair change in *BRO1* (resulting in a C359Y change) that was present in defective progeny but not in the parental SEY6210 *hse1Δ* strain. Sanger sequencing confirmed this difference (Figure 1B).

Residue 359 of Bro1 lies within the linker region between the N-terminal Bro1 homology domain and the middle V domain. Importantly, the SF838-9D parental strain has normal MVB and vacuolar protease sorting pathways despite having the *BRO1* Y359 allele. However, a *bro1Δ* deletion has a typical “class E” Vps phenotype (Raymond et al., 1992), indicating that a sorting defect results only when the Y359-encoding allele of *BRO1* is combined with loss of *HSE1*. As confirmation, we made homozygous *hse1Δ* diploids from SF838-9D and SEY6210, in which the *BRO1* gene was knocked out of either haplotype. The *hse1Δ* diploids having only the Y359 Bro1 from SF838-9D showed a strong MVB sorting defect as assessed by the localization of Sna3-GFP (Figure 1C), a well-characterized MVB cargo (Macdonald et al.,

2012b). In contrast, *hse1Δ* homozygotes with the SEY6210 allele of *BRO1* (C359) sorted Sna3-GFP normally. Although the biochemical defects of the Y359 Bro1 mutant were not investigated, the value of this mutant was to help uncover the genetic interaction between Bro1 and ESCRT-0.

To confirm the synthetic genetic interaction between Bro1 and Hse1, we analyzed MVB sorting in SEY6210 *bro1Δ* cells that also contained defined mutations in ESCRT-0 (Figure 1D). Loss of Bro1 blocked the delivery of Ste3-GFP to the vacuole lumen, causing these cells to accumulate large “class E” endosomal compartments. Interestingly, other cargoes could still be sorted to the vacuole of *bro1Δ* cells, albeit to a limited degree. Both Ste3-GFP-Ub (an in-frame fusion of Ub on to Ste3-GFP) and GFP-tagged Mup1 (a methionine transporter) were sorted moderately well in *bro1Δ* cells and normally in *hse1Δ* cells. Combined loss of *HSE1* and *BRO1* caused substantial sorting defects that were observed by microscopy (Figure 1D) and by immunoblotting for a GFP fragment (Figure S1B), which is cleaved from cargo upon delivery into the vacuolar lumen (Hetzema et al., 2004). A synthetic defect was also observed when the *bro1Δ* mutation was combined with a hypomorphic mutation in Vps27 that blocks the ability of ESCRT-0 to bind to clathrin (*vps27^{Δchc1}*) (Bilodeau et al., 2003; Shields et al., 2009). Finally, we found that levels of Bro1 were unperturbed by alterations in ESCRT-0 and that levels of ESCRT-0 subunit Vps27 were unperturbed by changes in *BRO1* or *HSE1*, indicating that the synthetic interaction between Bro1 and ESCRT-0 functions is specific (Figure S1C).

Bro1 Acts Early in Cargo Sorting and Binds Clathrin

The synthetic genetic interaction between Bro1 and ESCRT-0 suggested that Bro1 may act early in the MVB sorting process in parallel with ESCRT-0. This function would be distinct from that previously established for Bro1, which is to recruit the Doa4 DUB to ESCRT-III to remove Ub from MVB cargo and rescue Ub from excessive vacuolar degradation and which is mediated by Bro1 binding to Snf7 via its N-terminal Bro1 domain and Doa4 via its proline-rich C-terminal domain (Amerik et al., 2006; Nikko and André, 2007; Richter et al., 2007). Previous studies show that fusing the catalytic domain of a DUB onto ESCRT-0 effectively deubiquitinates cargo “early” in the sorting process, thereby blocking delivery to the vacuolar lumen (MacDonald et al., 2012a; Stringer and Piper, 2011). This block can be circumvented by translationally fusing Ub to the C termini of cargo, making it resistant to the effects of ESCRT-DUB fusions. We reasoned that if Bro1 also could intervene early in the sorting process in parallel to ESCRT-0, then a Bro1-DUB fusion protein should also block cargo sorting to the vacuole and not merely replace the Bro1:Doa4 complex thought to work postsorting to simply recycle Ub. Fusions of Bro1 to the catalytic domain of Ubp7 or UL36 (a yeast cysteine-based Ub-specific protease or a DUB found within the tegument protein of herpes simplex virus-1, respectively) were expressed in wild-type cells (Figure 2A). In addition to causing defective sorting of Ste3 and Sna3, Bro1-Ubp7 and Bro1-UL36 also perturbed sorting of Gap1 and Fur4 (the general amino acid permease and uracil permease). In contrast, Ste3-GFP-Ub, containing an in-frame fusion of Ub that cannot be removed by DUBs, sorted normally, demonstrating that Bro1-Ubp7 and Bro1-UL36 exert their

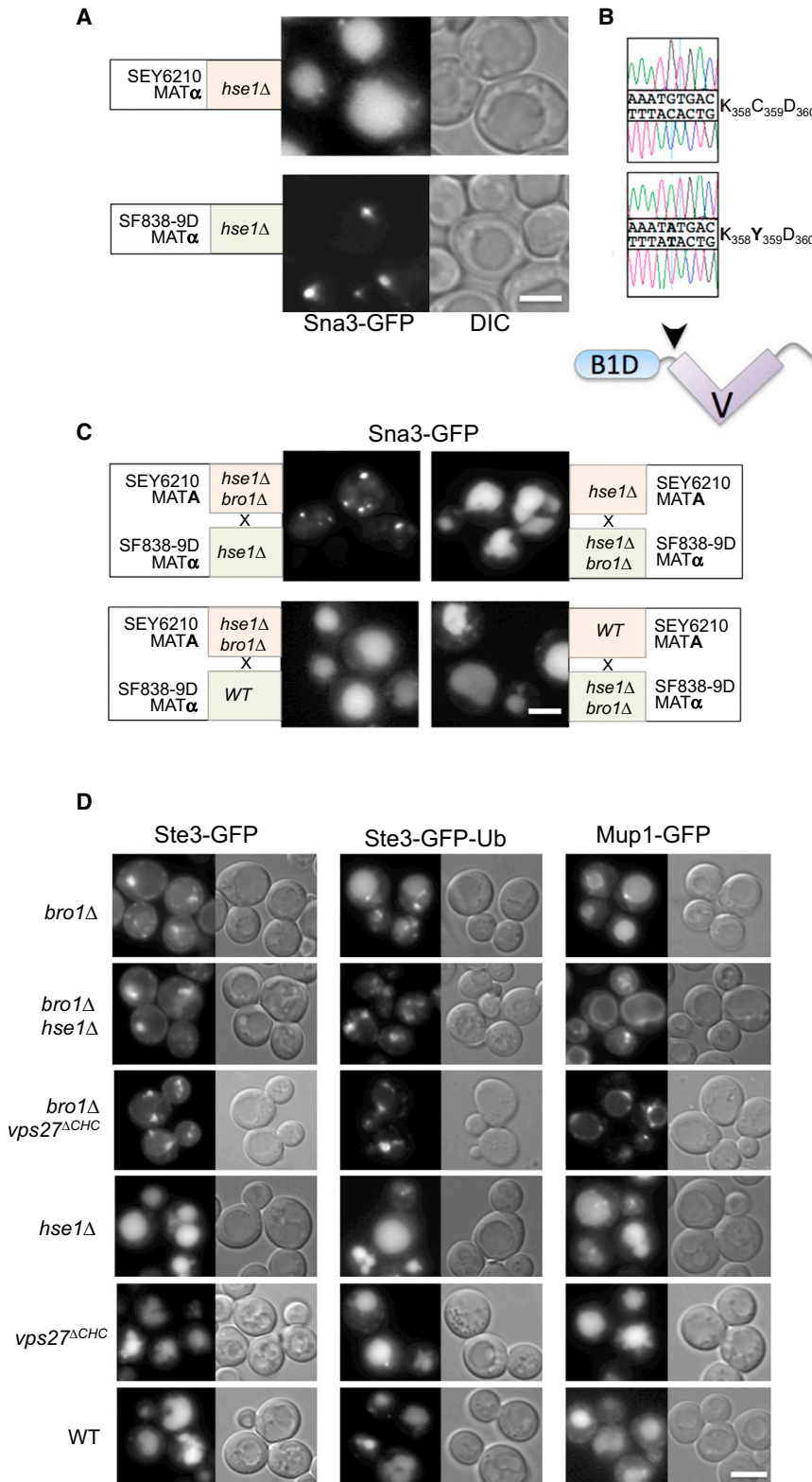


Figure 1. Synthetic Interaction between Bro1 and ESCRT-0

(A) Localization of Sna3-GFP in *hse1* Δ null mutants generated from the SEY6210 and SF838-9D parental strains. Shown are differential interference contrast (DIC) and GFP fluorescence images. (B) Chromatograms of *BRO1* open reading frame sequence (Sanger sequencing of PCR-amplified DNA) from SEY6210 cells (top) or SF838-9D cells (bottom). Arrowhead in schematic below indicates location of residue 359 between the N-terminal Bro1 homology domain (B1D) and the middle V domain.

(C) Demonstration that the *bro1*^{Y359} allele causes a synthetic phenotype with *hse1* Δ . *BRO1* was disrupted in MAT(A) SEY6210 *hse1* Δ or MAT α SF838 *hse1* Δ haploids, and these were subsequently mated to form diploids. Sorting of Sna3-GFP to the vacuole lumen was defective in *hse1* Δ homozygous diploids with only the *bro1*^{Y359} allele from the SF838-9D haplotype. However, Sna3-GFP was correctly sorted in *hse1* Δ homozygous diploids with only *BRO1*^{C359} from the SEY6210 haplotype. Diploids heterozygous for both *hse1* Δ *bro1* Δ also sorted Sna3-GFP properly regardless of either haplotype.

(D) Localization of Ste3-GFP, Ste3-GFP-Ub, and Mup1-GFP in SEY6210 cells of the indicated genotypes: WT; *bro1* Δ null alone; *bro1* Δ *hse1* Δ double null; *Vps27* lacking its C-terminal clathrin-binding motif (*vps27* ^{Δ^{Chc1}}); *hse1* Δ alone or the *vps27* ^{Δ^{Chc1}} mutation alone. Scale bar, 5 μ m.

See also Figure S1 and Tables S1 and S2.

of Bro1 (Figure 1D), suggesting that Bro1 may normally operate on a subset of MVB cargos.

The effect of Bro1-DUB in blocking cargo sorting is not due simply to recruiting DUB activity to ESCRT-III. We found that expressing a fusion of UL36 to the Microtubule Interacting and Trafficking (MIT) domain of Vps4, which interacts with MIT-Interaction Motifs within ESCRT-III subunits (Obita et al., 2007; Stuchell-Brereton et al., 2007), did not affect MVB cargo sorting (Figure 2B). However, MIT-UL36 as well as UL36 fusion to full-length Bro1 and just the N-terminal Bro1 domain prevented the delivery of GFP-Ub into the vacuole, demonstrating that these proteins could stimulate recycling of Ub from cargo before it was consumed in the MVB sorting process. Thus, the dominant effect of Bro1-DUB proteins on the sorting of particular cargos likely reflects a

inhibitory effect at the level of deubiquitinating cargo rather than altering the function of ESCRT apparatus itself. Mup1-GFP was only modestly affected by the Bro1-DUB fusions (Figure 2A) and also underwent some level of MVB sorting, even in the absence

function of Bro1 that works early in the cargo sorting process (Figure 2C).

One of the biochemical features of ESCRT-0 and other proposed ESCRT-0-like Ub-sorting receptors such as Tom1 and

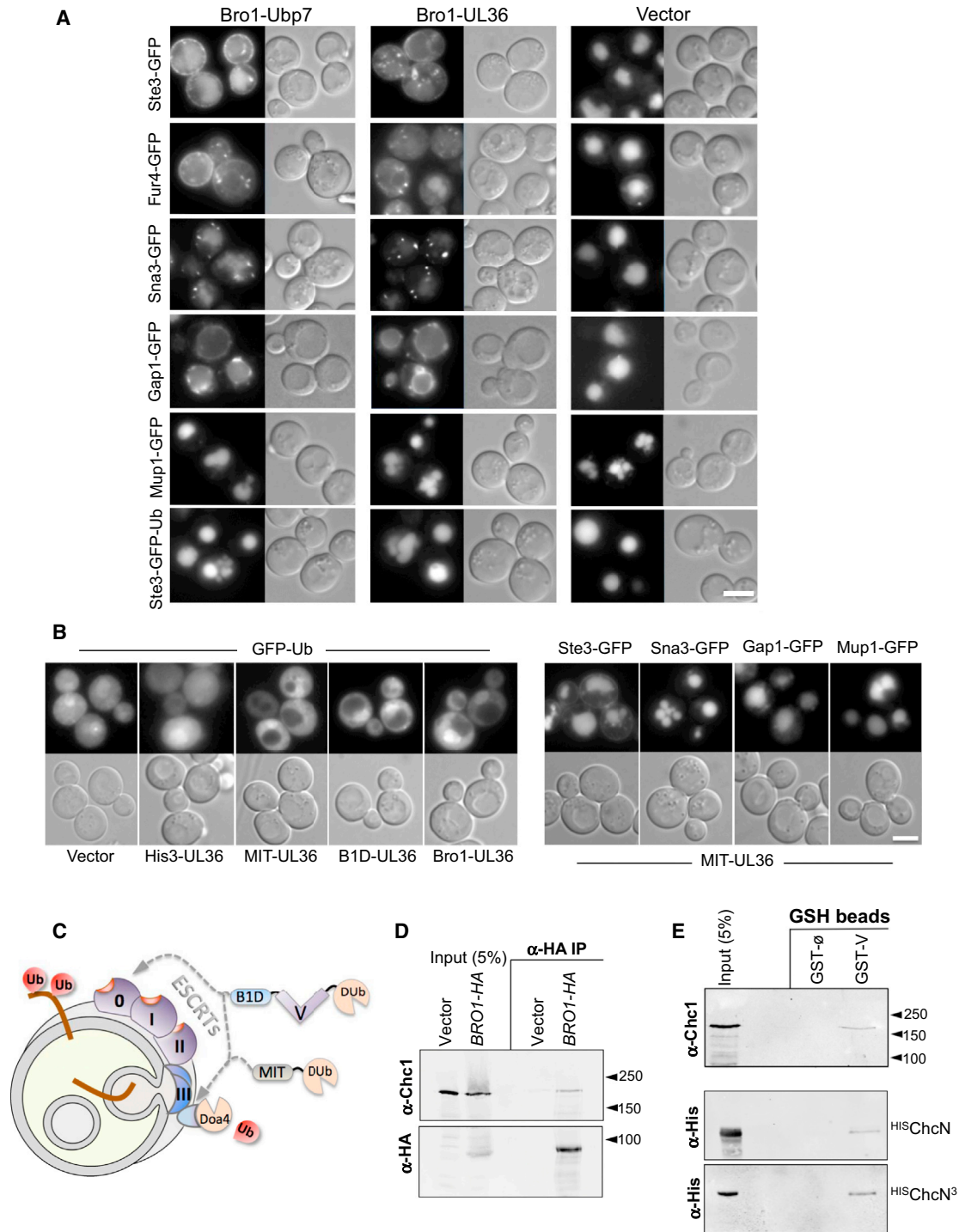


Figure 2. Effect of Bro1-DUB Fusion Protein on the Sorting of MVB Cargo

(A) Bro1 fusion proteins containing the catalytic domain of either Ubp7 (Bro1-Ubp7) or UL36 (Bro1-UL36) were expressed from the copper-inducible *CUP1* promoter in WT cells, in combination with the indicated GFP-tagged MVB cargo proteins. Shown are DIC and GFP fluorescence images.

(B) Left: sorting of GFP-Ub in WT cells or in cells expressing the UL36 fused to His3 (His3-UL36), the N-terminal MIT domain of Vps4 (MIT-UL36), the N-terminal Bro1 domain (B1D-UL36), or full-length Bro1 (Bro1-UL36) (left). WT cells or cells expressing a His3-UL36 fusion protein accumulate some GFP-Ub within vacuoles. Expression of Bro1-UL36 or MIT-UL36 excludes GFP-Ub from vacuoles. Right: MIT-UL36 was also coexpressed in WT cells with the indicated GFP-tagged MVB cargo. Scale bar, 5 μ m

(C) Model for how Bro1 might work in two places: early in the process of cargo sorting in conjunction with ESCRT-0, such that the Bro1-DUB fusion proteins deubiquitinate cargo and block subsequent sorting into the MVB pathway; and late in the sorting process in conjunction with ESCRT-III, to recycle Ub from the MVB pathway and thus prevent its accumulation in the vacuole. This latter function can be mimicked by MIT-DUB.

(legend continued on next page)

GGAs is that they bind clathrin, which is found in distinct endosomal subdomains that concentrate Ub-cargo and help localize ESCRT-0 (Shields and Piper, 2011). Coimmunoprecipitation experiments showed that Bro1 shares the ability of ESCRT-0 to associate with clathrin in vivo (Figure 2D). Clathrin-binding activity was housed within the middle Bro1 V domain since a glutathione S-transferase (GST)-V domain fusion protein was sufficient to pull down clathrin from yeast lysates (Figure 2E). Also, the recombinant N-terminal β -propeller domain of clathrin heavy chain could specifically bind GST-V, indicating that the Bro1 V domain binds directly to clathrin (Figure 2E). Interestingly, Bro1 has a conserved clathrin binding box motif (ter Haar et al., 2000) within an unstructured loop at the vertex of its V domain (Figures S2A and S2B). However, mutations in this region did not block coimmunoprecipitation of Bro1 with clathrin from cell lysates, suggesting that other motifs may also be sufficient for clathrin association (data not shown).

The V Domains of Bro1 Family Proteins Bind Ub

One of the key features of ESCRT-0 that allows it to act as a sorting receptor for Ub-cargo is its ability to bind Ub. Recently, the Bro1 homolog Alix was found to bind Ub via its middle V domain (Joshi et al., 2008). The Alix V domain is organized into two trihelical bundles adopting the shape of a V with a short and long arm (Fisher et al., 2007; Lee et al., 2007). We found that the V domains of Bro1, Rim20, human Alix, and HD-PTP bind directly to Ub even though they share only a moderate level of sequence identity. This was demonstrated by the ability of recombinant V domains to bind a Ub-GST fusion protein (Figure 3A) and to bind K63-linked polyubiquitin (poly-Ub) chains (Figure 3B).

Chemical shift perturbations measured by nuclear magnetic resonance (NMR) heteronuclear single quantum coherence (HSQC) experiments with ^{15}N -Ub showed that the Bro1 V domain bound mono-Ub (Figures 3C, S3A, and S3B) and used a binding surface centered on the hydrophobic patch of Ub that comprised I44, V70, L8, and R42 (Figure 3D), which serves as a common surface engaged by the vast majority of Ub-binding proteins (Husnjak and Dikic, 2012). These experiments utilized the V domain from *S. castelli* Bro1, which shares 56% identity with *S. cerevisiae* Bro1 V but had better stability in vitro. The Alix V domain also bound mono-Ub through the same general surface patch, although the profile of chemical shift perturbations in ^{15}N -Ub induced by Alix V binding was slightly different, indicating a different binding mode (Figure 3D; Figures S3A and S3B). Significant line broadening was evident for all peaks of ^{15}N -Ub with increasing concentrations of V domains (Figure S3C). This was most severe for His-domain protein tyrosine phosphatase (HD-PTP) V domain, which precluded the ability to use chemical shift changes to map the interface on Ub. The NMR peaks from Ub bound to V domain were likely broadened because the Ub-V complex is much larger than Ub alone and in range of intermediate exchange on the NMR time-

scale. Using loss of peak intensity as a measure of binding estimates the dissociation constant, K_D , of the V domains of Alix and HD-PTP in the range of $\sim 50\ \mu\text{M}$ and the *S. castelli* Bro1 V domain ~ 5 times higher.

To map the major Ub-binding site on Bro1 V in solution, we performed a series of paramagnetic relaxation enhancement (PRE) experiments using a set of Bro1 V mutants containing a nitroxide spin label (methanethiosulfonate [MTSL]) attached to cysteine residues substituted at different positions (Figure 3E). MTSL-labeled Bro1 V proteins were used in HSQC experiments with ^{15}N -Ub in the presence and absence of ascorbate. The oxidized form of the attached MTSL enhances the relaxation rate of nearby spin systems, resulting in a loss of peak intensity in HSQC spectra as compared to the ascorbate-reduced form that has lost its unpaired electron (Iwahara and Clore, 2006). Significant PRE effects on any of the residues of ^{15}N -Ub were plotted for each of the labeled Bro1 V variants (Figure 3F), revealing dramatic effects for spin labels incorporated in the N-terminal helix of first trihelical arm of the Bro1 V domain at residues 381 and 392. As confirmation, we generated a “half-V” protein that comprised only the first trihelical arm and found that it bound Ub in GST pull-down assays and induced a profile of chemical shift perturbations on the surface ^{15}N -Ub similar to that of full-length Bro1 V (Figures S3D–S3I).

Further structural information about Ub binding was obtained through protein crystallography experiments yielding a structure of Ub bound to the first trihelical arm the *S. castelli* Bro1 V domain. This structure was solved from crystals containing a selenomethionine-labeled Bro1V:Ub A28M complex diffracting to $3.6\ \text{\AA}$ that allowed us to use the single-wavelength anomalous dispersion method to obtain experimental phases (Table 1). Two V domains were found in the asymmetric unit with five selenium sites per molecule of V domain. Despite the low level of sequence homology, the Bro1 V domain was remarkably similar to the Alix V domain, each with two trihelical arms with the protein sequence crisscrossing between the two arms. Unlike Alix V, the two arms of Bro1 V were of similar size (Figure 4A), and the relative orientation of the trihelical arms and the helices within the distal C-terminal arm as they twist through the arm were different.

Ub was bound to one of the V domains (Chain A) within the asymmetric unit (Figures 4B, S4A, and S4B), where it was positioned along residues 375–386 of the exposed inner surface of the N-terminal trihelical bundle, in direct agreement with the PRE experiments placing residue 381 near the major site of Ub binding in solution. Ub was oriented along the N-terminal V domain helix so that the C terminus of Ub was near the opening of the V domain and the N terminus of Ub was pointing toward the vertex of the V domain. The binding surface in Ub that was identified by chemical shift perturbations in NMR HSQC experiments (including residues L8, I44, and V70) was oriented toward the Bro1 V N-terminal helix (Figure 4B). To confirm the

(D) Immunoprecipitation of HA-tagged Bro1 from spheroplasts prepared from cells transformed with vector alone or plasmid expressing Bro1-HA. Samples were immunoblotted with monoclonal antibodies against Cbc1 (top) or HA (bottom).

(E) Pull-down of GST alone (GST- \emptyset) or GST fused to the Bro1 V domain (GST-V). Bead-bound fractions were immunoblotted as was a 5% equivalent of input. Top: pull-down of Cbc1 from yeast lysates. Bottom: pull-down of a monomeric 6xHis-tagged recombinant N-terminal clathrin β -propeller (^{35}S CbcN) or an oligomeric version containing a trimerization domain (^{35}S CbcN 3).

See also Figure S2 and Tables S1 and S2.

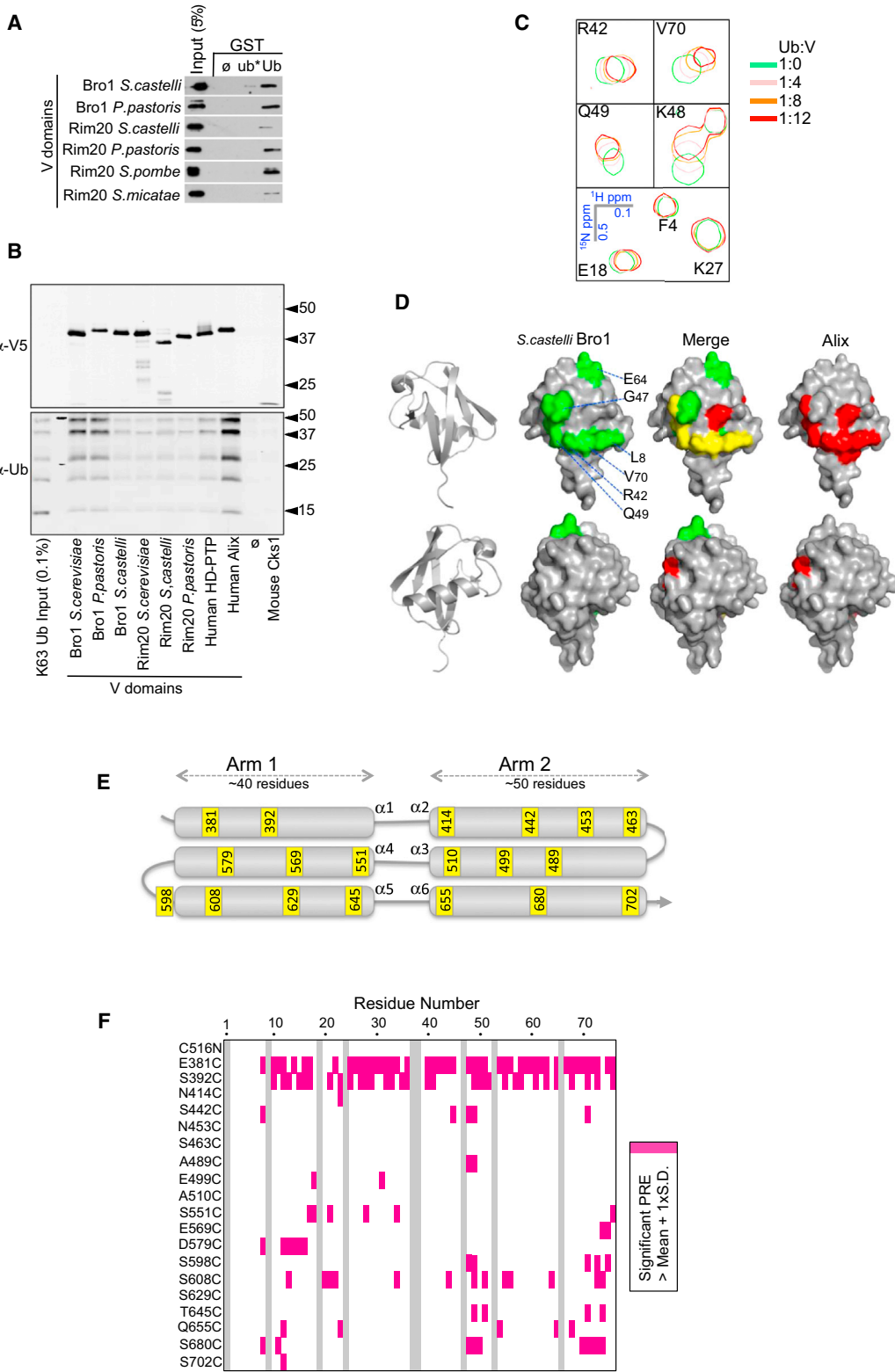


Figure 3. V Domains of Bro1 and Other Family Members Bind Ub

(A) GST pull-down experiments of recombinant Bro1 and Rim20 V domains *S. castelli*, *P. pastoris*, *S. pombe*, and *S. micatae* using GST alone (GST- \emptyset), GST fused to Ub (Ub), or a mutant Ub with mutations in L8, I44, R42, and V70 (ub*).

(B) Recombinant V domains were immobilized on α -V5 polyclonal antibody-coated beads, washed, and incubated with K63-linked polyubiquitin chains. Beads, alone or bound to an irrelevant V5-epitope-tagged protein, were also included. Beads were washed and immunoblotted with α -V5 or α -Ub monoclonal antibodies.

(legend continued on next page)

low-resolution crystal structure, we made an additional spin-labeled Bro1 V domain with MTSL attached to the first residue of the V domain (residue 369) and compared its PRE profile on ^{15}N -Ub to a Bro1 V domain spin labeled at residue 392. The differential PRE effect between these two site-specific spin labels on the backbone amides of Ub showed that residue 369 of Bro1 V was nearer to the C terminus of Ub, while 381 was nearer to the N-terminal region of Ub (Figure S4C). Together, these data demonstrate that Ub lies along the first alpha helix of the Bro1 V domain in an antiparallel orientation and indicate that I377 likely participates in hydrophobic interactions with L8, I44, and V70 of Ub.

V Domains Adopt an Open Conformation in Solution

The structure of Bro1 V (Figure 4) and previous structures of Alix V domains show a relatively closed conformation that might restrict access of some YPxL-containing proteins or ubiquitinated proteins to their binding sites on the inner surface (Fisher et al., 2007; Lee et al., 2007). Indeed, full-length Alix forms an intramolecular interaction (between its C-terminal proline-rich domain and its N-terminal Bro1 homology domain), which diminishes binding to YPxL-containing proteins. This interaction may function as a clasp, holding the V domain in a closed conformation that, upon release, allows the V domain to spring open to expose protein interaction sites (Pires et al., 2009; Zhai et al., 2011; Zhou et al., 2010). We obtained several lines of evidence demonstrating that, in the absence of such a clasp, the V domain adopts an open conformation in solution. Small angle X-ray scattering (SAXS) data from monodisperse Bro1 and Alix V domains were used to generate *ab initio* envelopes and revealed elongated V domains that were splayed open relative to their crystal structures (Figures 5A and S5A). These elongated shapes were consistent with gel filtration data and dynamic light scattering, showing that the monomeric 40 kDa Alix V and the 36 kDa of Bro1 V domains behaved as larger forms (Figures S5C–S5E).

Attempts to crystallize Alix V in complex with Ub yielded a 6.5 Å crystal structure of Alix V in an open conformation without clear electron density for Ub (Figure 5C; Table 1). The single wavelength anomalous dispersion technique with isomorphous crystals of seleniomethionine-labeled Alix V allowed us to locate the selenium sites, determine phases, and obtain traceable electron density maps. The features in the electron density maps clearly matched details in other Alix V structures; however, the angle between the two arms of Alix V was far greater (e.g., an open conformation) than that found for the previously determined closed conformations (Figure 5D; Movie S1). Having both the open and closed crystal structures of Alix V and the closed structure of Bro1 V allowed us to calculate experimental

fit to the SAXS data of isolated V domains in solution. This analysis (Figure S5B) showed that the SAXS data best describe a mix of V domains in both open and closed forms at a ratio of roughly 50:50.

The large shape changes displayed by V domains prompted us to test whether they might undergo more dramatic changes in solution involving the swapping of N- and C-terminal helices between the trihelical bundles. We engineered a tobacco etch virus (TEV) protease site in the middle hinge region of the V domain so that, if a swap did occur, the protein could separate into two roughly equal fragments. However, cleaved Bro1 V stayed intact assessed by gel filtration even after extended incubation at 25°C (Figure S5F).

Together, these data show that, while the overall topology of V domains is retained in solution, they can undergo a variety of conformational changes, with small-scale changes evident in the packing of the helices within Bro1 V crystals (Figure S4A) and large-scale changes in a mix of open and closed forms in solution (Figure 5).

Ub Binding by Bro1 Is Required for MVB Sorting of Ub-Cargo

To test the functional relevance of Ub binding by Bro1, we generated mutants of Bro1 V domain specifically defective in binding Ub. A series of mutations within the first trihelical arm were tested for their ability to disrupt Ub binding using PRE experiments with ^{15}N -Ub and Bro1 V mutants spin labeled at position 381. Although side chains cannot be resolved with the diffraction data in the crystal structure, I377 is predicted from our structural data to be centered under the hydrophobic patch of Ub, whereas L386 lies under a loop region between $\alpha 2$ and $\beta 5$ of Ub containing residues Q62, K63, E64, and S65. We found that mutation of I377 and/or L386 blocked Ub binding as observed by the loss of PRE effect in ^{15}N Ub (Figure 6A). Loss of Ub binding was also indicated by a loss in chemical shift perturbations in the backbone amides of Ub residues that mediate binding to Bro1 V (Figure 6B) and by loss of the ability of Bro1 V domains immobilized on beads to bind K63 poly-Ub chains (Figure 6C). Compared to the wild-type (WT) Bro1 V protein, the mutant V domains were produced at similar levels, were just as soluble, and had identical NMR proton spectra (Figure S6), indicating that the mutant V domains retained their overall structure.

We next assessed the ability of Bro1 containing Ub-binding-defective V domains to sort cargo into the MVB pathway (Figure 7). Here we analyzed chimeric Bro1 proteins in which the V domain of a hemagglutinin (HA)-epitope-tagged Bro1 from *S. cerevisiae* was substituted with the mutant V domains of *S. castelli* characterized earlier. The WT chimeric Bro1-HA was

(C) HSQC NMR spectra of indicated backbone amides of 30 μM ^{15}N -Ub in the absence and presence of the *S. castelli* V domain at the designated ratios.

(D) Significant chemical shift perturbations [>1 SD of $(0.2\text{N}^2 + \text{H}^2)^{1/2}$] caused by binding of the Bro1 or Alix V domain to ^{15}N -Ub in HSQC experiments were mapped onto the molecular surface of Ub. Shown are front and back views of Ub, with the binding surface for Bro1 in green and Alix in red. Overlap in the two chemical shift perturbation profiles is shown as yellow in the merge.

(E) Schematic of the *S. castelli* V domain, which forms two trihelical arms. The amino acid positions in yellow designate cysteine substitutions used to conjugate site-specific spin labels using MTSL.

(F) Summary of paramagnetic relaxation experiments using the series of Bro1 cysteine mutants that bear spin label at the indicated positions. The NMR $^{15}\text{N}/^1\text{H}$ HSQC spectra of 30 μM ^{15}N -Ub with 100 μM of the indicated MTSL-labeled Bro1 V domains were collected in the presence (oxidized) and absence (reduced) of 2 mM ascorbate. Peak intensity ratios of these two spectra were calculated for each backbone amide. Plot of Ub residues that were subject to significant PRE, as reflected by a significant reduction in peak intensity ratio, are defined as >1 SD above the mean for that residue across the whole data set.

See also Figure S3 and Table S1.

Table 1. Crystallography Statistics

Statistics	SeMet Bro1V ^{SEM} :	
	UbA28M	SeMet AlixV:Ub
Data Collection		
Space group	P2 ₁ 2 ₁ 2 ₁	I23
Unit cell parameters (Å)	a = 63.43, b = 92.32, c = 229.45	a = b = c = 223.77
Resolution (Å)	34.49–3.50 (3.62–3.50)	39.56–6.50 (6.73–6.50)
R _{merge}	8.4 (61.1)	6.1 (74.8)
Unique reflections	17,664 (1,700)	3,774 (370)
< I/σ(I) >	6.6 (1.7)	23.3 (2.1)
Completeness (%)	100.0 (99.9)	100.0 (100.0)
Multiplicity	7.1 (7.3)	21.4 (22.3)
Anomalous < I/σ(I) >	5.3 (1.0)	18.6 (1.2)
Anomalous completeness (%)	99.9 (99.9)	100.0 (100.0)
Anomalous multiplicity	3.85 (3.83)	11.4 (11.6)
Refinement		
Resolution (Å)	34.49–3.60	39.56–6.50
Number of reflections	16,053	3,760
R _{work} /R _{free}	36.6/42.1	20.3/28.3
Number of protein atoms	3,536	5,398
B Factors		
Wilson (Å ²)	131.3	468.9
Average (Å ²)	158.2	150.3
Root-Mean-Square Deviations		
Bond lengths (Å)	0.002	0.002
Bond angles (°)	0.665	0.550
Molprobit Statistics		
Ramachandran favored (%)	91.2	90.6
Allowed (%)	7.4	8.2
Outliers (%)	1.31	1.2
All-atom clash score	4.27	4.79
Overall score	1.72	2.01
Solvent content (%)	68.5	78.5
Molecules of V domain/ asymmetric unit	2	2

These crystallography statistics are given for an open conformation of the human Alix V domain (PDB ID: 4JJY) and a crystal structure of the yeast Bro1 V domain in a complex with Ub (PDB ID: 4JIO).

produced at levels identical to those of full-length *S. cerevisiae* Bro1-HA and complemented the MVB sorting defects (Figures 7A and S7). Two Ub-binding-defective mutants of Bro1 (Bro1^{ΔUBD1}, I377R; and Bro1^{ΔUBD2}, L386R) also complemented *bro1Δ* mutants and were able to sort Ste3-GFP and Ste3-GFP-Ub into the vacuole, although modest defects were observed for Ste3-GFP sorting by the Bro1^{ΔUBD2} mutant. Their level of expression was identical to WT Bro1-HA and not affected by *hse1Δ* or *vps27^{ΔChc1}* mutations (Figure S7). These data demonstrate that the Bro1 mutants retain their general folding and function. We reasoned that if Bro1—and, in particular, the Ub-binding capacity of Bro1—functions in parallel with ESCRT-0

as a Ub-sorting receptor, then the functional defects of Bro1^{ΔUBD1} and Bro1^{ΔUBD2} would be compensated for by ESCRT-0. Thus, we analyzed the ability of Bro1^{ΔUBD1} and Bro1^{ΔUBD2} to mediate MVB sorting in cells where ESCRT-0 was compromised by either loss of Hse1 or loss of clathrin binding to Vps27. Notably, *hse1Δ* mutants and *vps27^{ΔChc1}* mutants have no phenotype on their own; also, double mutants with *bro1* (*bro1Δ hse1Δ* and *bro1Δ vps27^{ΔChc1}*) were complemented for MVB sorting by Bro1-HA with the WT V domain. In contrast, sorting of Ste3-GFP was markedly defective when either of the Bro1^{ΔUBD1} and Bro1^{ΔUBD2} alleles was combined with the *vps27^{ΔChc1}* allele or loss of Hse1 (Figures 7B and 7C). Severe sorting defects were also observed for Ste3-GFP-Ub. More moderate defects were observed when Bro1^{ΔUBD1} and Bro1^{ΔUBD2} combined with the *vps27^{ΔChc1}* allele, which may reflect that loss of clathrin binding compromises ESCRT-0 function less than loss of Hse1. Both the Bro1^{ΔUBD1} and Bro1^{ΔUBD2} proteins were able to restore carboxypeptidase Y (CPY) sorting to not only *bro1Δ* mutants but also the *bro1Δ hse1Δ* and *bro1Δ vps27^{ΔChc1}* mutants, indicating that the deficiency caused by loss of Ub binding was specific to MVB sorting and not to all other Bro1 functions. In addition, we found that Bro1^{ΔUBD1} and Bro1^{ΔUBD2} cells had a normal distribution of GFP-tagged Ub, indicating that the Doa4 DUB was functioning normally to remove Ub from MVB cargo late in the process of sorting.

DISCUSSION

Based on the data presented here and elsewhere, we propose that Bro1 works early in the MVB biogenesis pathway, as a Ub-sorting receptor that functions in parallel with ESCRT-0. This role would be distinct from its later function as a recruitment factor for Doa4, the DUB that works late in the process of MVB biogenesis to recycle Ub from cargo postsorting (Amerik et al., 2006; Richter et al., 2007). This model is supported by the genetic interactions we observed between ESCRT-0 and Bro1, wherein hypomorphic mutations in both show dramatic synthetic phenotypes. Further support comes from the observation that expressing Bro1-DUB fusion proteins blocks the sorting of cargo into MVBs and from the finding that Bro1 shares several binding partners with ESCRT-0, including Ub, clathrin, ESCRT-I, Ub ligases, and DUBs (Nikko and André, 2007). These interactions provide a biochemical rationale for how Bro1 can execute an ESCRT-0-like function as a Ub-sorting receptor. We found that the interaction of the Bro1 V domain with Ub was critical for sorting Ub-cargo into MVBs only when ESCRT-0 function was weakened, an observation supporting the idea that Bro1 and ESCRT-0 provide similar overlapping functions. Interestingly, even when Ub-cargo sorting was blocked, other functions such as sorting of the soluble vacuolar hydrolase CPY were normal, demonstrating that the MVB and vacuolar hydrolase sorting functions of Bro1 are separable and that Ub binding contributes to the former.

Together, these data suggest that Bro1 belongs to an expanding coterie of endosomal Ub-sorting receptors, thereby diversifying membership beyond ESCRT-0, GGA, and Tom1-related proteins, which have a very similar domain organization (Clague et al., 2012; Shields and Piper, 2011). It is plausible that each of these Ub receptors directs its attention to specific sets of cargos

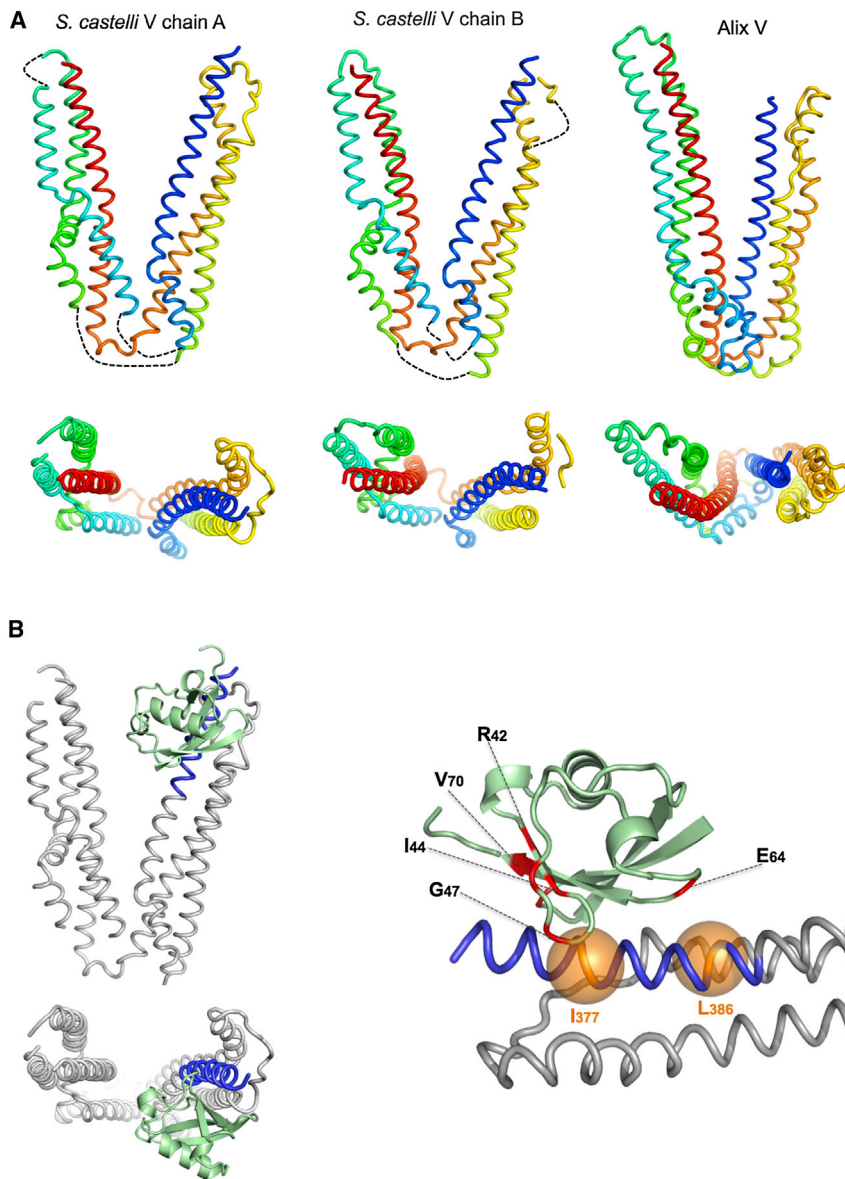


Figure 4. Crystal Structure of the Bro1 V Domain in Complex with Ub

(A) Structures (3.6 Å) of the Bro1 V domains found within the asymmetric unit (PDB ID: 4JIO). A cartoon model of the Alix V domain (PDB ID: 2OEX) is shown at right. Below is an alternate view from the top of the arms, looking into the vertex of the two Bro1 V domain structures together with Alix V. The backbone is colored blue-to-red according to amino acid order (N to C terminus). Loops not resolved in electron density maps are represented by dotted lines.

(B) Structure of the Ub:Bro1 V domain complex showing Ub (green) bound to the N terminus of the Bro1 V domain within the first trihelical bundle (residues 370–392, indicated in blue). Model at right is a closer view of Ub:V interaction. Ub residues that undergo significant NMR chemical perturbation upon Bro1 V binding are shown in red. Positions of the Bro1 V I377 and L386 C α atoms are shown in orange.

See also Figure S4 and Table S1.

with some level of overlap. This possibility is supported by our findings that loss of Bro1 or mutation of the Ub-binding site in the V domain leads to more dramatic defects in MVB sorting for cargos such as Ste3 than for others such as Mup1. If Bro1 does work as an upstream Ub-sorting receptor in the MVB biogenesis pathway, then the mammalian Bro1 family members Alix and HD-PTP may likewise execute such a function. Correspondingly, Alix was found to bind membrane proteins bearing YPXL motifs and to usher them into endosomal ILVs (Baietti et al., 2012; Dores et al., 2012). For one of these cargos (Par1), ubiquitination of the cargo itself was not required (although ubiquitination of associated proteins might be), suggesting that Alix can work as a sorting receptor for certain Ub-independent cargos. Since the Alix V domain binds Ub, it is possible that this protein also serves as a receptor for Ub-cargos. Unlike the loss of ESCRT-0 or ESCRT-I, loss of Alix in mammalian cells does not dramatically alter endosome

morphology, nor does it block sorting of the few ubiquitinated membrane protein cargos that have been examined (Odorizzi, 2006). Thus, Alix may handle only a subset of Ub-cargos, or ESCRT-0 could substitute for Alix's absence in experimental contexts. Interestingly, *Dictyostellium discoideum* does not have a canonical ESCRT-0 (Hrs/STAM) but does express a Bro1 homolog (Dd-Alix) and a Tom1 homolog (Dd-Tom1), the latter of which participates in many of the same protein interactions as a canonical ESCRT-0. Nevertheless, eliminating Dd-Tom1 affects neither the sorting of endosomal ubiquitinated proteins nor the biogenesis of MVBs, suggesting that Dd-Alix instead may provide much of the ESCRT-0-like function in this organism (Blanc et al., 2009).

Like both Alix and Bro1, HD-PTP also directly binds Ub, ESCRT-I, and ESCRT-III and localizes to endosomes (Doyotte et al., 2008; Miura et al., 2008; Nikko and André, 2007; Stefani et al., 2011; Strack et al., 2003). Loss of HD-PTP promotes cell migration and is associated with cancer progression (Cao et al., 1998; Castiglioni et al., 2007; Gilbert et al., 2011; Lin et al., 2011). At the cellular level, RNA interference (RNAi)-mediated depletion of HD-PTP causes morphological changes in endosomes and an accumulation of ubiquitinated proteins on them, a cellular phenotype similar to that resulting from ESCRT-0 depletion (Doyotte et al., 2008). Although it is not clear what types of Ub-cargo HD-PTP might sort, candidates include EGFR, integrins, and E-cadherin (Castiglioni et al., 2007; Lin et al., 2011; Miura et al., 2008).

Although we have speculated that other Bro1 family members can behave as endosomal Ub-sorting receptors, their capacity to bind Ub could instead be used for different or additional

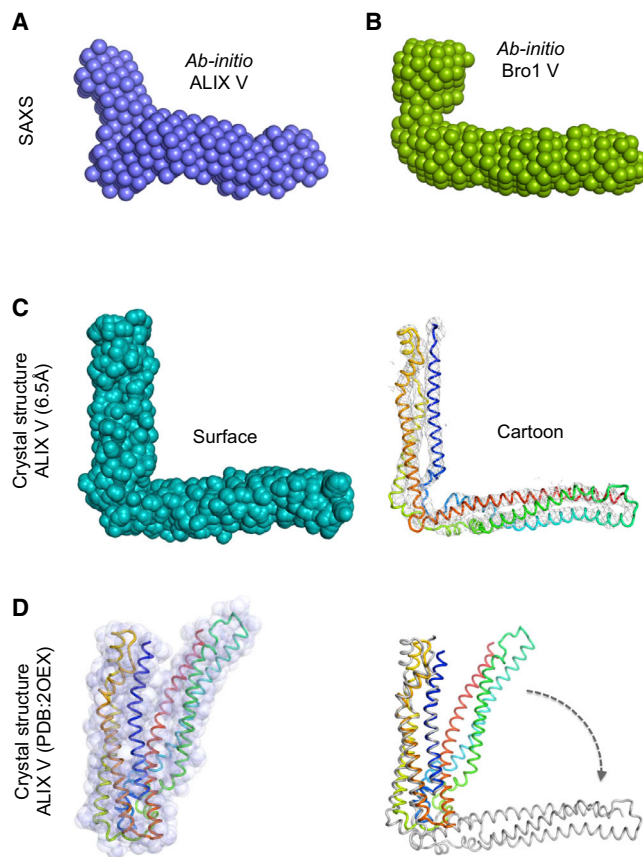


Figure 5. Alix and Bro1 V Domains in the Open Conformation

(A and B) Ab initio envelopes of (A) human Alix V domain and (B) the *S. castellii* Bro1 V domain, as determined by SAXS.

(C) Space-filling (left) and cartoon rendering (right) of the 6.5 Å crystal structure of human Alix V domain in an alternative open conformation (PDB ID: 4JJY). Experimental electron density contoured at 1 σ shown at left is shown as a gray mesh at right.

(D) Left: molecular surface and cartoon overlay of Alix V (PDB ID: 2OEX) in the closed conformation. Right: overlay of closed Alix V (colored) onto the open conformation of Alix V (gray) (right).

See also Figure S5, Table S1, and Movie S1.

purposes. For instance, many Ub-binding proteins, including Alix, can themselves undergo ubiquitination and may act as a scaffold for a variety of other Ub-binding proteins involved in endocytosis and/or viral budding (Hoeller and Dikic, 2010; Sette et al., 2010). In the future, such alternative models can be tested using Ub-binding-defective mutants of other Bro1 family proteins. Predicting how to generate such mutants will be somewhat challenging, however. Although the Ub-binding region we identified is conserved among Bro1 orthologs, how to accurately predict the Ub-binding site in the V domains of other proteins is not obvious. The V domains of HD-PTP, Alix, and Bro1 are only 13%–15% identical, and recent mutagenesis experiments indicate that Alix houses a UBD somewhere within its distal trihelical arm, along a sequence that is only conserved across Alix orthologs (Dowlatshahi et al., 2012; Keren-Kaplan et al., 2013). This theme of different Ub-binding modes between functional orthologs is found for components of the ESCRT apparatus as well;

Vps27 (ESCRT-0), Mvb12 (ESCRT-I), and Vps36 (ESCRT-II) share the ability to bind Ub with their mammalian counterparts Hrs, Mvb12A, UBAP1, and Eap45 but use different binding motifs to do so (Clague et al., 2012; Shields and Piper, 2011). This is consistent with the fact that low-affinity binding motifs for Ub are often structurally simple, suggesting they may not be that challenging to evolve.

EXPERIMENTAL PROCEDURES

Plasmids and yeast strains used are listed in Tables S1 and S2. *BRO1*-expressing plasmids with various V domains were made in low-copy/yeast centromere plasmids encoding the *BRO1* promoter and the flanking N-terminal and C-terminal portions of *S. cerevisiae* Bro1 upstream of two HA epitopes.

V domains produced in *E. coli* BL21(DE3) were purified over TALON-Co²⁺ and size exclusion chromatography and cleaved from their 6XHis tag with TEV protease prior to crystallography. Selenomethionine (SeMet)-labeled proteins were expressed using the methionine pathway inhibition procedure (Double and Carter, 1992).

Diffraction data were collected on the 4.2.2 beamline at the Advanced Light Source (Berkeley, CA, USA) on crystals containing Ub (A28M to allow labeling with selenium) and Bro1 V (with K417A, K418A, K419A mutations made to reduce surface entropy; Goldschmidt et al., 2007) or crystals of Alix. Data for SeMet-Bro1V:Ub (A28M) were processed using d*TREK (Pflugrath, 1999) and phased with phenix.autosol (Terwilliger et al., 2009) using the single-wavelength anomalous dispersion method. Phenix.autobuild and phenix.refine were used to iteratively build and improve the Bro1V C α -only model. Ub (Protein Data Bank [PDB] ID: 1UBQ) was docked into the clearly visible density near the Bro1V N terminus and refined with all atoms. The diffraction data for SeMet-AlixV:Ub were integrated and scaled using d*TREK and prepared for SHELXD (Sheldrick, 2008) using xprep (Bruker AXS, Madison, WI, USA). Phenix was used to improve the quality of the map sufficiently so that the two arms of AlixV from the high-resolution structures could be independently placed in the electron density and then refined with secondary structure restraints in place. Coot was used to manually fit the structure, and PyMOL was used to generate the structural figures.

SAXS data (collected at the 12-ID-B beamline at the Advanced Photon Source, Argonne National Laboratory, Argonne, IL, USA; and the SIBYLS 12.3.1 beamline at the Advanced Light Source, Lawrence Berkeley National Laboratory, Berkeley, CA, USA) were processed with PRIMUS (Konarev et al., 2003). The radius of gyration (R_g) estimated from Guinier plots was 34.3 Å for Alix V and 35.4 Å for Bro1 V. The maximum diameter (D_{max}) determined with GNOM was 116.0 Å and 111.1 Å for Alix and Bro1 V domains, respectively. The ab initio models were generated with GASBOR (Svergun et al., 2001). FoXS, along with its Minimal Ensemble Search algorithm, was used to calculate weighted fit of the open and closed forms of V domains (Schneidman-Duhovny et al., 2010).

¹⁵N-HSQC data were collected at 25°C on a Bruker Avance II 800 MHz spectrometer and analyzed with SPARKY (T.D. Goddard and D.G. Kneller, SPARKY 3, University of California, San Francisco, San Francisco, CA, USA) and NMRView (One Moon Scientific, Westfield, NJ, USA). Chemical shift perturbations were measured by comparing peak positions to ¹⁵N-Ub alone using $(0.2 \Delta \text{ppm}^2 + \Delta \text{ppm}^2)^{1/2}$. Paramagnetic relaxation enhancement effects were measured using cysteine-containing Bro1 proteins labeled with MTSL [(1-oxyl-2,2,5,5-tetramethylpyrrolidine-3-methyl)-methanethiosulfonate] (Toronto Research Chemicals, Toronto, Ontario, Canada). Incorporation to >90% was validated by electron spin resonance analysis. Peak intensity ratios of ¹⁵N-Ub when bound to the oxidized versus reduced MTSL-labeled Bro1 proteins were calculated to quantify the degree of PRE effects.

GFP-fusion proteins were localized in cells grown to mid-log phase at 30°C and imaged as previously described (Bilodeau et al., 2003). Genes under control of the *CUP1* promoter were induced with 50 μ M CuCl₂. Yeast protein extracts for immunoblotting were prepared as described elsewhere (Kushnirov, 2000). GST pull-down experiments and immunoprecipitations were done as described previously (Bilodeau et al., 2003; Pashkova et al., 2010). Binding to K63 poly-Ub was done by attaching recombinant 6xHis-V5-tagged V domains to 30 μ l of beads coated with polyclonal anti-V5 antibodies, which

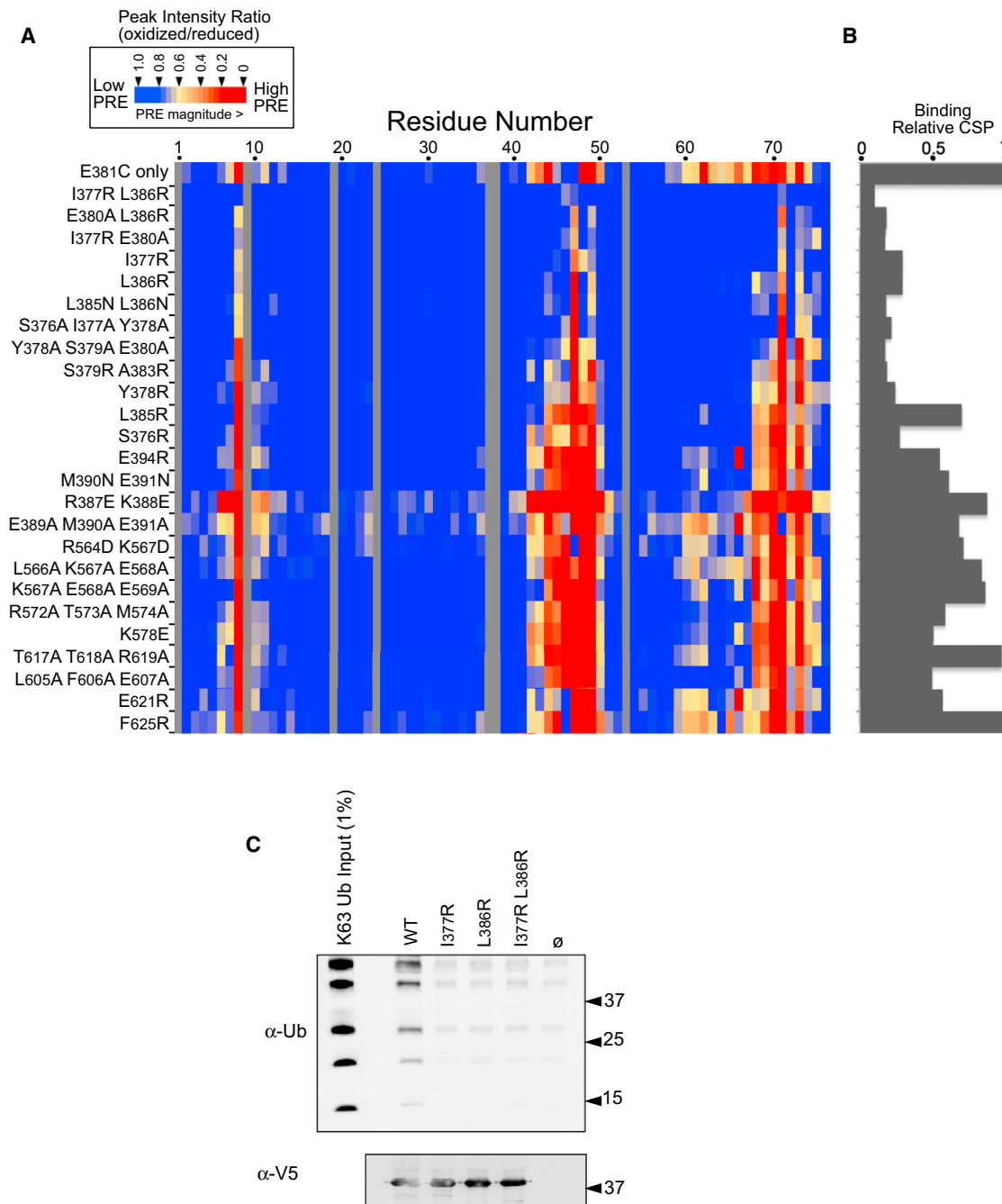


Figure 6. Mutagenesis of the Ub-Binding Region of Bro1 V Domain

(A) The indicated mutations were made in the context of the *S. castelli* Bro1 domain, which contains a cysteine residue at position 381. These proteins were labeled with MTSL and used in PRE experiments with ¹⁵N-Ub at a Bro1 V:Ub ratio of 3:1. Peak intensity ratios (oxidized versus reduced spin label) for each Ub residue were calculated from HSQC spectra collected in the absence and presence of 2 mM ascorbate. The degree of PRE effect experienced by each Ub backbone amide is color coded as indicated.

(B) Index of chemical-shift perturbations in ¹⁵N-Ub upon binding to mutant Bro1 V domains. Chemical shift perturbation (CSP) index was calculated by summing the $(0.2\Delta N^2 + \Delta H^2)^{1/2}$ values for Ub residues 8, 42, 44, 48, 49, 69, 70, and 71 and setting that value equal to 1 for the WT Bro1 V domain.

(C) The WT and mutant recombinant V domains were immobilized on α-V5 polyclonal antibody-coated beads, washed, and incubated with K63-linked poly-ubiquitin chains. Beads alone or bound to an irrelevant V5-epitoped protein were also included. Beads were washed and immunoblotted with α-V5 or α-Ub monoclonal antibodies.

See also Figure S6 and Table S1.

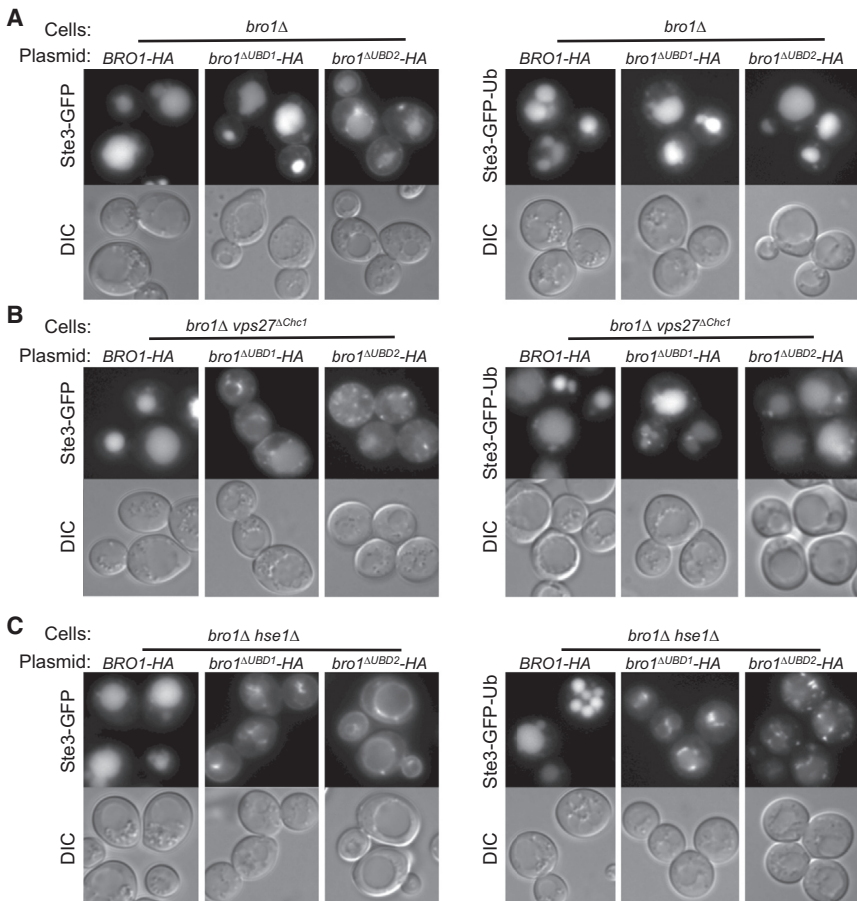


Figure 7. MVB Sorting Requires Bro1 to Bind Ub

(A) Null mutant *bro1Δ* cells were transformed with low-copy-number plasmids expressing a WT chimeric Bro1 with the V domain from *S. castelli* Bro1, with or without mutations in the Ub-binding region of the V domain. The *bro1^{ΔUBD1}* allele carries the I377R mutation; *bro1^{ΔUBD2}* carries the L386R mutation. Cells also expressed Ste3-GFP (left) or Ste3-GFP-Ub (right). Shown are GFP fluorescence and DIC images.

(B) Same as in (A), but *bro1Δ* cells also carried the *vps27^{ΔChc1}* allele that blocks the ability of Vps27 to bind directly to clathrin.

(C) Same as in (A) but *bro1Δ* cells also lack the ESCRT-0 subunit Hse1. Scale bar, 5 μm.

See also Figure S7 and Tables S1 and S2.

were subsequently incubated for 1 hr with 2 μg of K63-linked poly-Ub (Boston Biochemicals, Cambridge, MA, USA) in 200 μl PBS containing 0.02% of Triton X-100, 0.1% bovine serum albumin or casein. Beads were washed five times; bound complexes were eluted with Laemmli sample buffer and heating to 70°C for 5 min.

To compare yeast genomic DNA, 7–9 million 75-base-pair, single-end reads were generated for each sample on a HiSeq 2000 platform machine (Illumina, San Diego, CA, USA). Data were analyzed by the University of Washington Genome Sciences group as detailed in the [Supplemental Experimental Procedures](#).

ACCESSION NUMBERS

The structures of the Bro1 V:Ub complex and an open conformation of Alix V have been deposited in the Protein Data Bank under ID codes 4JIO and 4JJY, respectively.

SUPPLEMENTAL INFORMATION

Supplemental Information includes Supplemental Experimental Procedures, seven figures, two tables, and one movie and can be found with this article online at <http://dx.doi.org/10.1016/j.devcel.2013.04.007>.

ACKNOWLEDGMENTS

This work was supported by National Institutes of Health (NIH) Grant GM58202. We thank Ernesto Fuentes for SAXS data collection and preliminary analysis. X-ray scattering beam time resource was provided at beamline 12-ID-B at the Advanced Photon Source. Analysis of yeast genomic sequences

was made possible through the NIH P41 GM103533 grant funding the Yeast Resource Center. M.J.D. is supported as a Rita Allen Scholar. A.B.S. was supported by National Cancer Institute Grant F30 CA165440 and National Institute on Aging Grant T32 AG000057.

Received: December 10, 2012

Revised: March 8, 2013

Accepted: April 9, 2013

Published: May 30, 2013

REFERENCES

- Amerik, A.Y., Nowak, J., Swaminathan, S., and Hochstrasser, M. (2000). The Doa4 deubiquitinating enzyme is functionally linked to the vacuolar protein-sorting and endocytic pathways. *Mol. Biol. Cell* *11*, 3365–3380.
- Amerik, A., Sindhi, N., and Hochstrasser, M. (2006). A conserved late endosome-targeting signal required for Doa4 deubiquitylating enzyme function. *J. Cell Biol.* *175*, 825–835.
- Babst, M., Davies, B.A., and Katzmann, D.J. (2011). Regulation of Vps4 during MVB sorting and cytokinesis. *Traffic* *12*, 1298–1305.
- Baietti, M.F., Zhang, Z., Mortier, E., Melchior, A., Degeest, G., Geeraerts, A., Ivarsson, Y., Depoortere, F., Coomans, C., Vermeiren, E., et al. (2012). Syndecan-syntenin-ALIX regulates the biogenesis of exosomes. *Nat. Cell Biol.* *14*, 677–685.
- Bilodeau, P.S., Urbanowski, J.L., Winistorfer, S.C., and Piper, R.C. (2002). The Vps27p Hse1p complex binds ubiquitin and mediates endosomal protein sorting. *Nat. Cell Biol.* *4*, 534–539.
- Bilodeau, P.S., Winistorfer, S.C., Kearney, W.R., Robertson, A.D., and Piper, R.C. (2003). Vps27-Hse1 and ESCRT-I complexes cooperate to increase

- efficiency of sorting ubiquitinated proteins at the endosome. *J. Cell Biol.* **163**, 237–243.
- Blanc, C., Charette, S.J., Mattei, S., Aubry, L., Smith, E.W., Cosson, P., and Letourneur, F. (2009). Dictyostelium Tom1 participates to an ancestral ESCRT-0 complex. *Traffic* **10**, 161–171.
- Cao, L., Zhang, L., Ruiz-Lozano, P., Yang, Q., Chien, K.R., Graham, R.M., and Zhou, M. (1998). A novel putative protein-tyrosine phosphatase contains a BRO1-like domain and suppresses Ha-ras-mediated transformation. *J. Biol. Chem.* **273**, 21077–21083.
- Castiglioni, S., Maier, J.A., and Mariotti, M. (2007). The tyrosine phosphatase HD-PTP: A novel player in endothelial migration. *Biochem. Biophys. Res. Commun.* **364**, 534–539.
- Clague, M.J., Liu, H., and Urbé, S. (2012). Governance of endocytic trafficking and signaling by reversible ubiquitylation. *Dev. Cell* **23**, 457–467.
- Dores, M.R., Chen, B., Lin, H., Soh, U.J., Paing, M.M., Montagne, W.A., Meerloo, T., and Trejo, J. (2012). ALIX binds a YPX(3)L motif of the GPCR PAR1 and mediates ubiquitin-independent ESCRT-III/MVB sorting. *J. Cell Biol.* **197**, 407–419.
- Double, S., and Carter, C. (1992). *Crystallization of Nucleic Acids and Proteins: A Practical Approach* (Oxford, UK: IRL Press).
- Dowlatshahi, D.P., Sandrin, V., Vivona, S., Shaler, T.A., Kaiser, S.E., Melandri, F., Sundquist, W.I., and Kopito, R.R. (2012). ALIX is a Lys63-specific polyubiquitin binding protein that functions in retrovirus budding. *Dev. Cell* **23**, 1247–1254.
- Doyotte, A., Mironov, A., McKenzie, E., and Woodman, P. (2008). The Bro1-related protein HD-PTP/PTPN23 is required for endosomal cargo sorting and multivesicular body morphogenesis. *Proc. Natl. Acad. Sci. USA* **105**, 6308–6313.
- Fisher, R.D., Chung, H.Y., Zhai, Q., Robinson, H., Sundquist, W.I., and Hill, C.P. (2007). Structural and biochemical studies of ALIX/AIP1 and its role in retrovirus budding. *Cell* **128**, 841–852.
- Gilbert, M.M., Tipping, M., Veraksa, A., and Moberg, K.H. (2011). A screen for conditional growth suppressor genes identifies the *Drosophila* homolog of HD-PTP as a regulator of the oncoprotein Yorkie. *Dev. Cell* **20**, 700–712.
- Goldschmidt, L., Cooper, D.R., Derewenda, Z.S., and Eisenberg, D. (2007). Toward rational protein crystallization: A Web server for the design of crystallizable protein variants. *Protein Sci.* **16**, 1569–1576.
- Hanson, P.I., and Cashikar, A. (2012). Multivesicular body morphogenesis. *Annu. Rev. Cell Dev. Biol.* **28**, 337–362.
- Henne, W.M., Buchkovich, N.J., and Emr, S.D. (2011). The ESCRT pathway. *Dev. Cell* **21**, 77–91.
- Hettema, E.H., Valdez-Taubas, J., and Pelham, H.R. (2004). Bsd2 binds the ubiquitin ligase Rsp5 and mediates the ubiquitination of transmembrane proteins. *EMBO J.* **23**, 1279–1288.
- Hoeller, D., and Dikic, I. (2010). Regulation of ubiquitin receptors by coupled monoubiquitination. *Subcell. Biochem.* **54**, 31–40.
- Husnjak, K., and Dikic, I. (2012). Ubiquitin-binding proteins: decoders of ubiquitin-mediated cellular functions. *Annu. Rev. Biochem.* **81**, 291–322.
- Iwahara, J., and Clore, G.M. (2006). Detecting transient intermediates in macromolecular binding by paramagnetic NMR. *Nature* **440**, 1227–1230.
- Joshi, A., Munshi, U., Ablan, S.D., Nagashima, K., and Freed, E.O. (2008). Functional replacement of a retroviral late domain by ubiquitin fusion. *Traffic* **9**, 1972–1983.
- Keren-Kaplan, T., Attali, I., Estrin, M., Kuo, L.S., Farkash, E., Jerabek-Willemsen, M., Blutraich, N., Artzi, S., Peri, A., Freed, E.O., et al. (2013). Structure-based in silico identification of ubiquitin-binding domains provides insights into the ALIX-V:ubiquitin complex and retrovirus budding. *EMBO J.* **32**, 538–551.
- Kim, J., Sitaraman, S., Hierro, A., Beach, B.M., Odorizzi, G., and Hurley, J.H. (2005). Structural basis for endosomal targeting by the Bro1 domain. *Dev. Cell* **8**, 937–947.
- Konarev, P., Volkov, V., Sokolova, A., Kocj, M., and Svergun, D. (2003). PRIMUS: a Windows PC-based system for small-angle scattering data analysis. *J. Appl. Crystallogr.* **36**, 1277–1282.
- Kushnirov, V.V. (2000). Rapid and reliable protein extraction from yeast. *Yeast* **16**, 857–860.
- Lee, S., Joshi, A., Nagashima, K., Freed, E.O., and Hurley, J.H. (2007). Structural basis for viral late-domain binding to Alix. *Nat. Struct. Mol. Biol.* **14**, 194–199.
- Lin, G., Aranda, V., Muthuswamy, S.K., and Tonks, N.K. (2011). Identification of PTPN23 as a novel regulator of cell invasion in mammary epithelial cells from a loss-of-function screen of the 'PTP-ome'. *Genes Dev.* **25**, 1412–1425.
- Luhtala, N., and Odorizzi, G. (2004). Bro1 coordinates deubiquitination in the multivesicular body pathway by recruiting Doa4 to endosomes. *J. Cell Biol.* **166**, 717–729.
- MacDonald, C., Buchkovich, N.J., Stringer, D.K., Emr, S.D., and Piper, R.C. (2012a). Cargo ubiquitination is essential for multivesicular body intraluminal vesicle formation. *EMBO Rep.* **13**, 331–338.
- Macdonald, C., Stringer, D.K., and Piper, R.C. (2012b). Sna3 is an Rsp5 adaptor protein that relies on ubiquitination for its MVB sorting. *Traffic* **13**, 586–598.
- Miura, G.I., Roignant, J.Y., Wassef, M., and Treisman, J.E. (2008). Myopic acts in the endocytic pathway to enhance signaling by the *Drosophila* EGF receptor. *Development* **135**, 1913–1922.
- Nikko, E., and André, B. (2007). Split-ubiquitin two-hybrid assay to analyze protein-protein interactions at the endosome: application to *Saccharomyces cerevisiae* Bro1 interacting with ESCRT complexes, the Doa4 ubiquitin hydrolase, and the Rsp5 ubiquitin ligase. *Eukaryot. Cell* **6**, 1266–1277.
- Obita, T., Saksena, S., Ghazi-Tabatabai, S., Gill, D.J., Perisic, O., Emr, S.D., and Williams, R.L. (2007). Structural basis for selective recognition of ESCRT-III by the AAA ATPase Vps4. *Nature* **449**, 735–739.
- Odorizzi, G. (2006). The multiple personalities of Alix. *J. Cell Sci.* **119**, 3025–3032.
- Odorizzi, G., Katzmann, D.J., Babst, M., Audhya, A., and Emr, S.D. (2003). Bro1 is an endosome-associated protein that functions in the MVB pathway in *Saccharomyces cerevisiae*. *J. Cell Sci.* **116**, 1893–1903.
- Pashkova, N., Gakhar, L., Winistorfer, S.C., Yu, L., Ramaswamy, S., and Piper, R.C. (2010). WD40 repeat propellers define a ubiquitin-binding domain that regulates turnover of F box proteins. *Mol. Cell* **40**, 433–443.
- Pflugrath, J.W. (1999). The finer things in X-ray diffraction data collection. *Acta Crystallogr. D Biol. Crystallogr.* **55**, 1718–1725.
- Pires, R., Hartlieb, B., Signor, L., Schoehn, G., Lata, S., Roessle, M., Moriscot, C., Popov, S., Hinz, A., Jamin, M., et al. (2009). A crescent-shaped ALIX dimer targets ESCRT-III CHMP4 filaments. *Structure* **17**, 843–856.
- Raymond, C.K., Howald-Stevenson, I., Vater, C.A., and Stevens, T.H. (1992). Morphological classification of the yeast vacuolar protein sorting mutants: evidence for a prevacuolar compartment in class E vps mutants. *Mol. Biol. Cell* **3**, 1389–1402.
- Ren, J., Pashkova, N., Winistorfer, S., and Piper, R.C. (2008). DOA1/UFD3 plays a role in sorting ubiquitinated membrane proteins into multivesicular bodies. *J. Biol. Chem.* **283**, 21599–21611.
- Richter, C., West, M., and Odorizzi, G. (2007). Dual mechanisms specify Doa4-mediated deubiquitination at multivesicular bodies. *EMBO J.* **26**, 2454–2464.
- Sadoul, R. (2006). Do Alix and ALG-2 really control endosomes for better or for worse? *Biol. Cell* **98**, 69–77.
- Sangsuriya, P., Rojtinakorn, J., Senapin, S., and Flegel, T.W. (2010). Identification and characterization of Alix/AIP1 interacting proteins from the black tiger shrimp, *Penaeus monodon*. *J. Fish Dis.* **33**, 571–581.
- Schneidman-Duhovny, D., Hammel, M., and Sali, A. (2010). FoXS: a web server for rapid computation and fitting of SAXS profiles. *Nucleic Acids Res.* **38**(Web Server issue), W540–W544.
- Sette, P., Jadwin, J.A., Dussupt, V., Bello, N.F., and Bouamr, F. (2010). The ESCRT-associated protein Alix recruits the ubiquitin ligase Nedd4-1 to facilitate HIV-1 release through the LYPXnLL domain motif. *J. Virol.* **84**, 8181–8192.

- Sheldrick, G.M. (2008). A short history of SHELX. *Acta Crystallogr. A* *64*, 112–122.
- Shields, S.B., and Piper, R.C. (2011). How ubiquitin functions with ESCRTs. *Traffic* *12*, 1306–1317.
- Shields, S.B., Oestreich, A.J., Winistorfer, S., Nguyen, D., Payne, J.A., Katzmann, D.J., and Piper, R. (2009). ESCRT ubiquitin-binding domains function cooperatively during MVB cargo sorting. *J. Cell Biol.* *185*, 213–224.
- Springael, J.Y., Nikko, E., André, B., and Marini, A.M. (2002). Yeast Npi3/Bro1 is involved in ubiquitin-dependent control of permease trafficking. *FEBS Lett.* *517*, 103–109.
- Stefani, F., Zhang, L., Taylor, S., Donovan, J., Rollinson, S., Doyotte, A., Brownhill, K., Bennion, J., Pickering-Brown, S., and Woodman, P. (2011). UBAP1 is a component of an endosome-specific ESCRT-I complex that is essential for MVB sorting. *Curr. Biol.* *21*, 1245–1250.
- Strack, B., Calistri, A., Craig, S., Popova, E., and Göttlinger, H.G. (2003). AIP1/ALIX is a binding partner for HIV-1 p6 and EIAV p9 functioning in virus budding. *Cell* *114*, 689–699.
- Stringer, D.K., and Piper, R.C. (2011). A single ubiquitin is sufficient for cargo protein entry into MVBs in the absence of ESCRT ubiquitination. *J. Cell Biol.* *192*, 229–242.
- Stuchell-Breton, M.D., Skalicky, J.J., Kieffer, C., Karren, M.A., Ghaffarian, S., and Sundquist, W.I. (2007). ESCRT-III recognition by VPS4 ATPases. *Nature* *449*, 740–744.
- Svergun, D.I., Petoukhov, M.V., and Koch, M.H. (2001). Determination of domain structure of proteins from X-ray solution scattering. *Biophys. J.* *80*, 2946–2953.
- ter Haar, E., Harrison, S.C., and Kirchhausen, T. (2000). Peptide-in-groove interactions link target proteins to the beta-propeller of clathrin. *Proc. Natl. Acad. Sci. USA* *97*, 1096–1100.
- Terwilliger, T.C., Adams, P.D., Read, R.J., McCoy, A.J., Moriarty, N.W., Grosse-Kunstleve, R.W., Afonine, P.V., Zwart, P.H., and Hung, L.W. (2009). Decision-making in structure solution using Bayesian estimates of map quality: the PHENIX AutoSol wizard. *Acta Crystallogr. D Biol. Crystallogr.* *65*, 582–601.
- Zhai, Q., Landesman, M.B., Chung, H.Y., Dierkers, A., Jeffries, C.M., Trewhella, J., Hill, C.P., and Sundquist, W.I. (2011). Activation of the retroviral budding factor ALIX. *J. Virol.* *85*, 9222–9226.
- Zhou, X., Si, J., Corvera, J., Gallick, G.E., and Kuang, J. (2010). Decoding the intrinsic mechanism that prohibits ALIX interaction with ESCRT and viral proteins. *Biochem. J.* *432*, 525–534.